Journal of Magnetic Resonance 212 (2011) 431–439

Contents lists available at SciVerse ScienceDirect

Journal of Magnetic Resonance

journal homepage: www.elsevier.com/locate/jmr

Site-specific ϕ- and ψ-torsion angle determination in a uniformly/extensively ^{13}C- and ^{15}N-labeled peptide

Sungsool Wi *, Justin Spano

Department of Chemistry, Virginia Polytechnic Institute and State University, Blacksburg, VA 24061, USA

ARTICLE INFO

Article history:
Received 20 May 2011
Revised 4 August 2011
Available online 17 August 2011

Keywords:
Solid-state NMR spectroscopy
Magic-angle spinning
Rotational-echo double resonance
Frequency-switched Lee–Goldburg decoupling
Lee–Goldburg cross-polarization
$^1H_\chi^C$–$^{15}N_2$ spin system

ABSTRACT

A solid-state rotational-echo double resonance (REDOR) NMR method was introduced to identify the ϕ- and ψ-torsion angle from a ^1H–^{15}N or ^1H–$^{13}C'$ spin system of alanine-like residues in a selectively, uniformly, or extensively ^{15}N-/^{13}C-labeled peptide. When a $C_\alpha(i)$ or a ^{15}N peak is site-specifically obtainable in the NMR spectrum of a uniformly ^{15}N/^{13}C-labeled sample system, the ψ- or ϕ-torsion angle specified by the conformational structure of peptide geometry involving $^{15}N(i)$–$^1H_\alpha i$–$^{15}N(i+1)$ or $^{13}C'(i-1)$–$^1H^N i$–$^{13}C'(i)$ spin system can be identified based on $^{13}C_\alpha$- or ^{15}N-detected $^1H_\alpha$–^{15}N or ^1H_N–^{13}C REDOR experiment. This method will conveniently be utilized to identify major secondary motifs, such as α-helix, β-sheet, and β-turn, from a uniformly ^{15}N-/^{13}C-labled peptide sample system. When tested on a ^{13}C-/^{15}N-labeled model system of a three amino acid peptide Gly–[U–^{13}C, ^{15}N]Ala–[U–^{13}C, ^{15}N]Leu, the ψ-angle of alanine obtained experimentally, $\psi = -40 \pm 30°$, agreed reasonably well with the X-ray determined angle, $\psi = -39°$.

1. Introduction

Solid-state nuclear magnetic resonance spectroscopy (SSNMR) has been utilized for investigating the conformational structures of biological solids. In particular, molecular torsion angles have been extracted by correlating two interacting, anisotropic tensors [1–10] or by measuring long-range, through-space distances [11–14] that constrain molecular torsion angles.

Among those tensor correlating methods, a seminary technique developed under high-resolution magic-angle spinning (MAS) conditions is NCCN–2Q HLF experiment [4] that measure the ψ-torsion angle around a C_α–C' bond by correlating the two C–N dipolar tensors in a peptide. Similarly, two C–H dipolar vectors were correlated around a C–C bond to measure the torsion angle involved in a HCCH molecular segment [3]. The NCCN–2Q HLF method is however insensitive to torsion angles less than ±120°, therefore, an alternative scheme, HCCN method [6] which correlates H_α–C_α dipolar vector and C'–N dipolar vector, has been developed for detecting a ψ-torsion angle less than |120°|. Also developed was to correlate H–N and H–C_α vectors to determine a ϕ-torsion angle along N–C_α bond [6]. Another type of correlation scheme developed for measuring ψ-torsion angle is the RACO method [7], which correlates the chemical shift anisotropy (CSA) of C' with the H_α–C_α dipolar vector in an amino acid residue. All these methods have limited applications because they require selective isotopic enrichments. Recently, a modified version of RACO method that is applicable to a uniformly ^{13}C labeled system has been developed [15]. An improved technique that uses the same spin topology as the RACO but can be applied to a uniformly/extensively labeled spin system is the ROCSA–LG [10], as the effect of C–C homonuclear dipolar coupling to CSA is minimized by the ROCSA sequence [16].

More involved techniques developed under MAS to measure both ϕ and ψ angles simultaneously are DQDRAWS [8] and DQCSA [9] methods. These methods correlate CSAs of two adjacent C' carbons in peptides. In DQDRAWS technique, the spinning sideband intensity of a C'–C' double quantum signal contains the mutual orientational information of C' CSA tensors. Compared with the DQDRAWS technique, the DQCSA method places fewer demands on the ^1H decoupling power and rf homogeneity. More sparse pulses are incorporated in the DQCSA pulse sequence with an indirect evolution time that is confined to a constant period of one or two rotor periods. Both DQDRAWS and DQCSA methods are suitable for selectively labeled peptides and are not affordable for uniformly or extensively labeled sample systems because of the presence of many ^{13}C–^{13}C homonuclear dipolar interactions.

A distance measurement between two nuclei, which are separated by more than three covalent bonds, constrains the torsion angle(s) involved along bonds connecting two nuclei. For instance, when the α-proton of C_α carbon is utilized, the $H_\alpha(i)$–$C'(i-1)$ and $H_\alpha(i)$–$N(i+1)$ distances will constrain the ϕ_i and ψ_i angles, respectively. These torsion angle dependent three-bond distances have been measured by $^2H_\alpha$–^{13}C or $^2H_\alpha$–^{15}N rotational-echo double

* Corresponding author. Fax: +1 540 231 3255.
E-mail address: sungsool@vt.edu (S. Wi).

1090-7807/$ - see front matter © 2011 Elsevier Inc. All rights reserved.
doi:10.1016/j.jmr.2011.08.019

resonance (REDOR) experiments by employing phase-modulated (PM) inversion pulses to ensure efficient inversion of $^2H_\alpha$ spins [17,18]. Hong and coworkers developed $^1H_N(i)$–$C'(i)$ and $^1H_\beta(i)$–$N(i)$ REDOR techniques for determining the $\phi(i)$ and side-chain torsion angle, $\chi(i)$, by incorporating a ^1H nucleus directly into the spin pair of distance measurements [14,19–21]. For a ^{13}C-/^{15}N-labeled peptide, a $^1H^Y$–X (Y is directly bonded to ^1H) REDOR method [19,20] was implemented for measuring the ^1H–X distance via Y detection, where X and Y are either a $^{13}C_\alpha$, $^{13}C_\beta$ or amide ^{15}N. The proton echo signal of a ^1H–X dipolar pair was recorded indirectly via a Y nucleus by applying a short Lee-Goldburg cross-polarization (LGCP) scheme [22,23] to prevents any potential signal contamination from the nearby protons via spin diffusion, while applying a series of π-pulses along the X channel for REDOR mixing. For encoding the ^1H echo signal during the REDOR evolution period, however, it is essential to remove strong ^1H–^1H homonuclear dipolar interactions by applying a homonuclear dipolar decoupling sequence, such as a frequency-switched Lee–Goldburg (FSLG) [24] or MREV-8 [25] sequence.

In this manuscript, we extended the $^1H^Y$–X REDOR approach and have examined various types of dipolar coupled spin systems involving H_α or H_N of alanine-like residues for determining ϕ- or ψ-torsion angles of major secondary structures in selectively, extensively, or even uniformly ^{13}C-/^{15}N-labeled peptides. Based on the indirect detection scheme along either C_α or N of an amino acid residue, spin systems that can be chosen for determining ϕ- or ψ-torsion angle determination include $H_\alpha(i)$–$N(i+1)$, $H_\alpha(i)$–$C'(i-1)$, and $H_N(i)$–$C'(i)$. For instance, a $^1H_\alpha(i)$–$^{15}N(i+1)$ is a very sensitive probe for determining the $\psi(i)$-torsion angle of a selectively labeled ith residue. When considered in an extensively/uniformly ^{15}N-labled system, the spin system is however dominated by the stronger $^1H_\alpha(i)$–$^{15}N(i)$ pair, which is invariant to the $\psi(i)$-torsion angle variation. Yet, an effectively isolated three-spin system, $^{15}N(i)$–$^1H_\alpha(i)$–$^{15}N(i+1)$, has been identified for differentiating major conformational structures possessing significantly different ψ angles, such as α-helix, β-sheets, and β-turns, etc.

2. Experiments

2.1. Materials

Natural abundance Gly–Ala–Leu and ^{13}C-/^{15}N-labeled Gly–[U–13C, ^{15}N]Ala–[U–13C, ^{15}N]Leu (labeling purity of both ^{13}C and ^{15}N: 98.0%) peptides were synthesized by Fmoc-based solid-state peptide synthesis at AnaSpec Inc. (San Jose, CA). The synthesized peptides were purified by reversed-phase liquid chromatography and the molecular weights of the purified peptides were confirmed by electrospray ionization mass analyzer. The labeled peptide, Gly–[U–13C, ^{15}N]Ala–[U–^{13}C, ^{15}N]Leu, was diluted to 18.0% in natural abundance Gly–Ala–Leu peptide, which was subsequently recrystallized according to the literature procedure [26]. About 46 mg of recrystallized peptide was center-packed into a 4 mm MAS rotor with bottom and top spacers. The sample temperature was kept constant at 22 °C by using BCU-X temperature control unit.

2.2. NMR pulse sequences

The NMR experiments were performed on a Bruker Avance II-300 NMR spectrometer (7.05 T) with Larmor frequencies of 30.41 MHz for ^{15}N, 75.47 MHz for ^{13}C, and 300.13 MHz for ^1H. Fig. 1A and B shows the pulse sequences used for our $^1H_\alpha^C$—^{15}N,$^1H_\alpha^C$—$^{13}C'$, or $^1H^N$–$^{13}C'$ REDOR experiments. The $^{13}C_\alpha$ or ^{15}N nuclei for signal encoding are initially irradiated using four $\pi/2$ pulses with 1 ms interpulse delay to remove the influence of any pre-existing transverse magnetizations. Equilibrium proton magnetizations are sent to a position in the xz-plane with an orientation of either $-35°$ or $145°$ with respect to z-axis before applying a frequency-switched Lee–Goldburg (FSLG) sequence along the x-axis with offsets, which removes ^1H–^1H homonuclear dipolar interactions during the evolution of ^1H echo signals for the REDOR mixing period. One rotor period (τ_r = 86.0 μs; ω_r = 11.635 kHz) of REDOR mixing time τ consists of four ($2\pi 2\bar{\pi}$) FSLG units, whose effective field strength is 93.08 kHz (ω_1 = 76 kHz) with offset $\Omega = \pm 53.74$ kHz. Two π-pulses per rotor period were applied along the indirect channel (for nitrogen channel, $\omega_1[^{15}N]$ = 26 kHz) to reintroduce ^1H–X (X = ^{15}N or $^{13}C'$) dipolar couplings under MAS. A π pulse (3 μs) is inserted in the middle of ^1H evolution to refocus the ^1H chemical shift. As noted in Fig. 1B, when both the irradiation and signal encoding are both along the carbon channel, a selective Gaussian pulse must be applied along the frequency range of C' around 170–180 ppm to ensure selective inversion of carbonyl peaks. A relevant mode of experiment that requires a selective Gaussian inversion is $^1H_\alpha^C$–$^{13}C'$ REDOR experiment.

For the $^1H_\alpha^C - ^{15}N$ REDOR experiment, a short (~150 μs) LGCP scheme (CP power: $\omega_1(^1H)$ = 50 kHz with offset =−35.4 kHz; $\omega_1(^{13}C)$ = 50 kHz) is employed for one-bond signal transfer from $^1H_\alpha$ to C_α for signal acquisition via ^{13}C channel. Spectra of 640–4096 scans were coadded with a recycle delay of 4 s. An extension to a two-dimensional (2D) $^{13}C/^{15}N$ correlation experiment is optional as included in Fig. 1A to increase the resolving power. ^1H $\pi/2$ and π pulse lengths were 2.5 and 5 μs, respectively, while ^{15}N π pulse length was 17.5 μs. A proton decoupling sequence, SPINAL-64, with ω_1 = 63 kHz is used during ^{13}C-detection for heteronuclear decoupling. Details of phase cycling steps are shown in the figure caption. REDOR dephasing signals (S) and reference signals (S_0) were recorded with and without irradiation of π pulses, respectively, along the indirect channel.

2.3. Simulation of REDOR dephasing curves

Since an analytical expression for the simulation of a REDOR dephasing curve fails to deal with real experimental conditions, such as finite pulse effects and relative tensor orientations involving multi-spin systems, brute-force calculations were carried out for an $I - S_n$ (n = 2 and 4) spin system using a in-house developed C^{++}-based program. A full density matrix evolution was considered under the influence of the REDOR π-pulses in the sequence. The program was developed to consider explicitly all the experimental parameters, such as pulse power, pulse duration, and spinning speed, and all the relevant internal tensor parameters, such as the magnitudes and relative orientations of $I - S_n$ dipolar interactions and chemical shift anisotropies (CSAs) of S (=^{15}N) spins. The I spin (=^1H) CSA tensor parameters are ignored in the actual calculation. The principal values of the amide nitrogen CSA tensor parameters used in the analysis were σ_{11} = 64 ppm, σ_2 = 77 ppm, and σ_{33} = 217 ppm [27]. All the relevant internal Hamiltonians are approximated as piecewise-constants with 60 increments per rotor period. Dipolar tensors and CSAs defined in their principal axis systems (PASs) transform to the laboratory frame (rotating frame in the usual sense) via multiple intermediate frames according to:

$$\begin{aligned}&\mathrm{CSA}(S_n, n = 2, \ldots) \overset{(\alpha_n^{CS}, \beta_n^{CS}, 0°)}{\rightarrow} \text{Dipolar interaction}\,(I - S_n)\\ &\times \overset{(0°, \theta_n, 0°)}{\rightarrow} \text{Dipolar interaction}\, I - S_1 \overset{(0°, \beta_1^d, \gamma_1^d)}{\rightarrow} \mathrm{CSA}(I)\\ &\times \overset{\text{powder angle}(\alpha,\beta,\gamma)}{\rightarrow} \text{Rotor Frame} \overset{(\omega_r t, 54.7°, 0°)}{\rightarrow} \text{Lab Frame}, \end{aligned} \quad (1)$$

where angle sets in the parenthesis are Euler angles transforming either a dipolar or CSA tensor from an old frame on the left side into a new frame on the right side of each transformation step in Eq. (1).

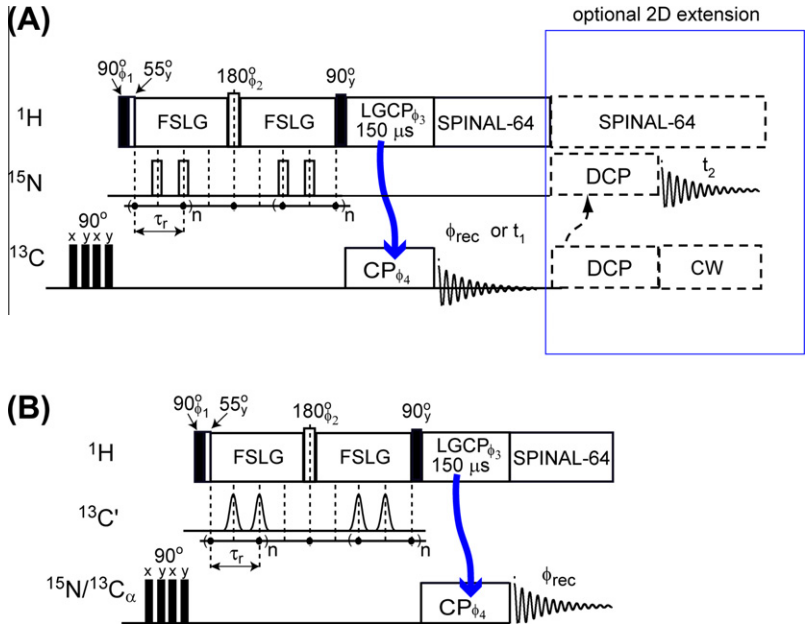

Fig. 1. Pulse sequences used for $^1H^Y$–X REDOR. Proton echo signals evolve during the REDOR mixing period under the FSLG sequence, which removes ^{1}H–^{1}H homonuclear dipolar interactions. FSLG decoupling power was 76 kHz, with eight 10.7 μs 294° rotation blocks per rotor period (τ_r = 86.0 μs), with offset frequencies of ±53.74 kHz. For the REDOR mixing period, either the $^1H_\alpha$ or ^1H_N echo signal evolves under two X-channel [^{15}N (A) or C′(B)] π-pulses per rotor period with XY-16 phase alternation scheme, and is transferred to a directly bonded Y [$^{13}C_\alpha$ (A) or ^{15}N (B)] using a short LGCP step (~150 μs) for detection. A 2D extension of the pulse sequence is optionally included in (A) to increase the resolving power of a spectrum on a standard 2D ^{13}C/^{15}N correlation scheme, utilizing a cross-polarization (CP) between $^{13}C_\alpha$ and ^{15}N or ^{13}C′ and ^{15}N. For inverting C′ nuclei selectively, a series of π-Gaussian pulses can be applied along the carbon channel (B). MAS was performed at 11.635 kHz spinning within ±1 Hz. Phase cycling: $\phi_1 = y, -y$; $\phi_2 = (y)_8, (-y)_8$; $\phi_3 = x$; $\phi_4 = x, x, -x, -x, y, y, -y, -y$; $\phi_{rec} = x, -x, -x, x, y, -y, -y, y$.

The relative tensor orientation between an I–S_n [$^1H_\alpha(i)$–$^{15}N(i+1)$, $^1H_\alpha(i)$–$^{15}N(i-1)$, or $^1H_\alpha(i)$–$^{15}N(i+2)$] vector and $I-S_1$ [$^1H_\alpha(i)$–^{15}N(i)] vector, θ_n, is instrumental in our REDOR analysis. However, the relative orientation between the CSA tensor of either a ^{1}H or ^{15}N and an $I-S_n$ dipolar vector was proven insignificant in REDOR dephasing characteristics (*vide infra*): $\alpha_n^{cs}, \beta_n^{cs}, \beta_1^d$, and γ_1^d angles were ignored in our actual analysis $\left(\alpha_n^{cs} = \beta_n^{cs} = \beta_1^d = \gamma_1^d = 0\right)$. Powder averages of REDOR dephasing signals were obtained by considering 11^3 crystallite orientations spanning over the powder angles α, β, and γ. The FSLG scaling factor, 0.57, was considered in our REDOR data analysis for evaluating a ^{1}H–^{15}N pair's dipolar coupling strength.

3. Spin systems consideration

3.1. $^1H_\alpha(i)$–$^{15}N(i+1)$, $^1H_\alpha(i)$–$^{13}C'(i-1)$, and $^1H^N(i)$–$^{13}C'(i)$ distances

These spin pair distances become basic distance constraints in our study that can be utilized for determining the $\phi(i)$- or $\psi(i)$-torsion angles in an alanine-like peptide geometry as shown in Fig. 2. The conformational degree of freedom in a $H_\alpha(i)$–$C_\alpha(i)$–C′(i)–N($i+1$) fragment is restricted by the rotation of ψ_H (=$\psi - 118^\circ$ angle (Fig. 2A). Therefore, the $^1H_\alpha(i)$–$^{15}N(i+1)$ distance varies according to the rotation of $\psi(i)$-angle as explained by the Supplementary Eq. (3) in the Supplementary information. In a typical alanine-like residue, the $H_\alpha(i)$–N($i+1$) distance will vary in the range of 2.38–3.29 Å (Fig. 2A).

The prediction of REDOR dephasing curves based on the calculated $H_\alpha(i)$–N($i+1$) distances obtained at $\psi(i)$-torsion angles of typical secondary structures is provided in Fig. 2A. Albeit the closeness in the dephasing curves between α-helix and 3_{10}-helix and between antiparallel and parallel β-sheet structures, the α-helix is clearly distinguishable from the β-sheet structure as they have clearly distinguishable $^1H_\alpha(i)$–$^{15}N(i+1)$ REDOR dephasing curves (Table 1). Additionally, it is predicted that the β-turn type-I and type-II structures are clearly distinguishable from each other. In all of our simulated REDOR dephasing curves, the FSLG scaling parameter, 0.577, has been considered explicitly in the simulations to estimate the dipolar strength of ^{1}H–X distances.

Likewise, a $^1H_\alpha(i)$–$^{13}C'(i-1)$ distance constrains $\phi_H(i)$-torsion angle (=$\phi(i) + 116^\circ$) in a molecular skeleton $H_\alpha(i)$–$C_\alpha(i)$–N(i –C′($i-1$). The $\phi(i)$-torsion angle dependent $^1H_\alpha(i)$–$^{13}C'(i-1)$ distances and the corresponding REDOR dephasing curves calculated based on the $H_\alpha(i)$–$C_\alpha(i)$–N(i)–C′($i-1$) geometry of the major secondary structures are shown in Fig. 2B. The variation range of $^1H_\alpha(i)$–$^{13}C'(i-1)$ distances is 2.5–3.3 Å [Fig. 2B; see Supplementary Eq. (4) in the Supporting Information]. Since the dipolar coupling strength of a $^1H_\alpha(i)$–$^{13}C'(i-1)$ pair is much stronger than that of $H_\alpha(i)$–N($i+1$), the calculated REDOR curves dephase more rapidly than those from $H_\alpha(i)$–N($i+1$) case. The $^1H_\alpha(i)$–$^{13}C'(i-1)$ REDOR analysis also distinguishes an α-helical structure against a β-sheet structure. In this case however the β-turn type-I and type-II structures provide an identical REDOR dephasing curve.

A $^1H^N(i)$–$^{13}C'(i)$ distance measurement is different from the previous two cases that it requires the signal encoding along the amide nitrogen. The $\phi_H{}^N(i)$-torsion angle rotation in the molecular segment, $H_N(i)$–N(i)–$C_\alpha(i)$–C′(i), provides a variation in the $^1H^N(i)$–$^{13}C'(i)$ distance (Fig. 2C) according to the Supplementary Eq. (5). The $\phi_H^N(i)$-torsion angle is related to the $\phi(i)$-torsion angle by $\phi_H^N(i) = \phi(i) + 180^\circ$. Sinha et al., utilized this mode of distance measurement for determining $\phi(i)$-torsion angle [12]. As shown in Fig. 2C, REDOR dephasing curves calculated based on the $^1H_N(i)$–$^{13}C'(i)$ distances are prominently different for α-helical and β-sheet structures. Moreover, this method offers sufficiently different REDOR dephasing curves for the parallel ($\phi = -119^\circ$) and anti-parallel ($\phi = -139^\circ$) β-sheet structures. As in the case of $^1H_\alpha(i)$–$^{13}C'(i-1)$, this mode does not distinguish β-turn type-I and -II structures either.

Additionally, for an amino acid residue that possesses a hydrogen atom in the β-carbon, such as isoleucine, valine, and threonine,

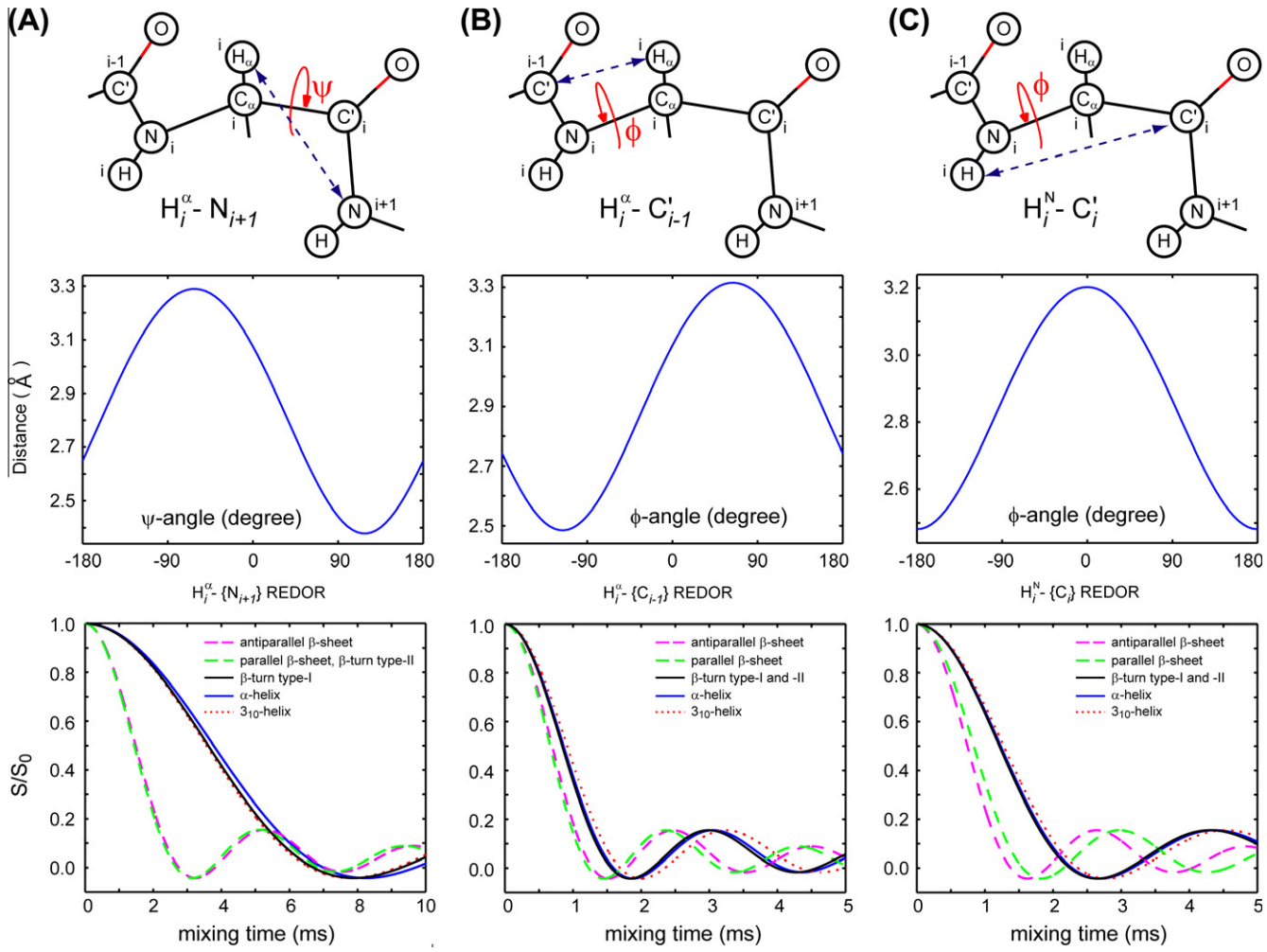

Fig. 2. (A) $^{1}H_{\alpha}(i)$–$^{15}N(i+1)$, (B) $^{1}H_{\alpha}(i)$–$C'(i-1)$, and (C) $^{1}H_{N}(i)$–$^{13}C'(i)$ distances in a peptide sequence consisting of alanine-like residues are obtained by varying either the $\psi(i)$- (A) or ϕ-torsion (B and C) angle. Parameters used as bond lengths and bond angles required to find these atom pair distances are provided in the Supporting Information. S/S_0 REDOR dephasing curves were simulated for ^{1}H–X (X = ^{15}N or $^{13}C'$) distances from α-helix, 3_{10}-helix, parallel and antiparallel β-sheets, and type-I and -II turns for each spin pair. The dipolar coupling strength of each spin pair was scaled down by the FSLG scaling factor (0.577). The universal REDOR dephasing curve was utilized for simulations.

Table 1
$^{1}H_{\alpha}$–^{15}N distances on peptide geometry determined by (ϕ, ψ) torsion angles defined over $i-1$, i, and $i+1$ residues involved in the sequences of major secondary structures.

	α-Helix	3_{10}-Helix	Antiparallel β-sheet	Parallel β-sheet	β-Turn type I	β-Turn type II
$\phi(i)$ (°)	−57	−49	−139	−119	−60	−60
$\psi(i)$ (°)	−47	−26	135	120	−30	120
$d[N(i)–N(i+1)] = d_1$ (Å)	2.78	2.65	3.52	3.42	2.67	3.42
$d[C'(i-1)–C'(i)] = d_2$ (Å)	3.00	2.94	3.62	3.50	3.02	3.02
$d[H_{\alpha}(i)–N(i+1)] = d_3$ (Å)	3.26	3.20	2.38	2.36	3.21	2.36
$d[H_{\alpha}(i)–C'(i-1)] = d_4$ (Å)	2.73	2.79	2.55	2.51	2.71	2.71
$d[H^{N}(i)–C'(i)] = d_5$ (Å)	3.20	3.25	2.65	2.77	3.19	3.19
$\angle[N(i)–H_{\alpha}(i)–N(i+1)]$[a] (°)	58	55	104	101	56	101
$\angle[C'(i-1)–H^{N}(i)–C'(i)]$[b] (°)	65	63	100	92	67	67

$d_6 = d[H_{\alpha}(i)–N(i)]$ and $d_7 = d[H^{N}(i)–C'(i-1)]$ are 2.08 Å and 2.04 Å for all cases.
[a] The $\angle[N(i)–H_{\alpha}(i)–N(i+1)]$ is identical to the angle θ defined in Fig. 2C.
[b] The $\angle[C'(i-1)–H^{N}(i)–C'(i)]$ is identical to the angle θ defined in Fig. 2A.

an additional molecular segment, $H_{\beta}(i)$–$C_{\beta}(i)$–$C_{\alpha}(i)$–$N(i)$, constrains the side-chain torsion angle χ_1 via the $H_{\beta}(i)$–$N(i)$ distance [12].

3.2. $^{15}N(i)$–$1H_{\alpha}(i)$–$^{15}N(i+1)$ and $C'(i-1)$–$^{1}H^{N}(i)$–$C'(i)$ spin systems

Although the angular precision of a torsion angle determination is highest when an isolated two-spin system is considered, the preparation of an isolated $^{1}H_{\alpha}(i)$–$^{15}N(i+1)$, $^{1}H_{\alpha}(i)$–$^{13}C'(i-1)$, or $^{1}H^{N}(i)$–$^{13}C'(i)$ spin system in a peptide sample requires an enrichment of a single, selectively ^{15}N- or $^{13}C'$-labeled amino acid residue by chemical synthesis. Usually it requires very expensive, elaborate efforts to prepare many differently labeled versions of well isolated spin pairs per a sample system for determining multiple ϕ- and ψ-torsion angles. Moreover, this approach is not applicable for protein samples prepared from bacterial growth. Thus, preparing a non-selective, multiply labeled sample system per a sample

based on a uniform or extensive labeling scheme reduces the cost, while maximizing the structural constraints. From a uniformly ^{13}C- and/or ^{15}N-labeled peptide or protein sample system, however, the spin systems become crowded, and the information contents coming from the longer dipolar pairs that are spanning over multiple covalent bonds are buried by the shorter dipolar pairs that are separated by one or two covalent bonds. This is because a stronger dipolar coupling interaction dominates the REDOR dephasing curve by overwhelming weaker dipolar coupling interactions in the spin network involved.

For a three-spin system that is composed of two heteronuclear dipolar interactions sharing a common nucleus, a minor modification by the weaker dipolar coupling to the REDOR dephasing curve that is predominantly determined by the stronger one may provide a still useful way for determining the major secondary structures in a uniformly or extensively ^{13}C-/^{15}N-labeled peptide or protein. For instance, a three-spin system, $^{15}N(i)$–$^{1}H_{\alpha}(i)$–$^{15}N(i+1)$, can be utilized to identify α-helical or β-sheet $\psi(i)$-torsion angles from a uniformly ^{13}C- and/or ^{15}N-labeled sample system. Other types of three-spin systems can be utilized are either a $C'(i-1)$–$1H^{N}(i)$–$C'(i)$ (Fig. 3B) or $C'(i-1)$–$1H_{\alpha}(i)$–$C'(i)$ that can be used to extract $\phi(i)$-torsion angle when a selective π-pulse irradiation scheme is employed for the 180° inversion of C′ carbons (Fig. 1B).

A three-spin system we have thoroughly investigated in this work is $^{15}N(i)$–$^{1}H_{\alpha}(i)$–$^{15}N(i+1)$ (Fig. 3A). The N(i) and N($i+1$) are separated from the $^{1}H_{\alpha}(i)$ atom by 2 and 3 bonds, respectively. While the $H_{\alpha}(i)$–N($i+1$) varies according to the rotation of $\psi_{H}(i) = \psi(i) - 118°$, the $H_{\alpha}(i)$–N(i) distance (2.08 Å) is invariant to the ψ_{H} angle rotation. An additional, nontrivial parameter that must be specified is the θ angle, $\angle$[N(i)–$H_{\alpha}i$ –$N(i+1)$], that varies also by the rotation of the ψ-torsion angle [28,29]. The dependence of the θ angle to the rotation of ψ-torsion angle is provided in Fig. 3A (see also the Supporting information). The angle θ defined between the $H_{\alpha}(i)$–N(i) and $H_{\alpha}(i)$–N($i+1$) dipolar vectors varies in the range of 54.5–104.2° as the ψ-torsion angle rotates along $C_{\alpha}i$–$C'(i)$ bond (Fig. 3A). For example, for a peptide geometry having ψ = 120° (parallel β-sheet), the θ angle and the $H_{\alpha}(i)$–N($i+1$) distance required for constraining the this torsion angle are θ = 99.6° and d[H_{α}–N($i+1$)] = 2.38 Å, respectively.

Fig. 3A shows a three-dimensional (3D) plot of the simulated $^{15}N(i)$–$^{1}H_{\alpha}(i)$–$^{15}N(i+1)$ S/S_0 REDOR dephasing curves generated based on the fixed $H_{\alpha}(i)$–N(i) coupling strength, which works as a control, and the variable $H_{\alpha}(i)$–N($i+1$) coupling strength and θ defined between two dipolar vectors as the ψ-torsion angle varies from −180° to 180° ($\psi_{H} = \psi - 118°$). Here, it must be noticed that the angular degeneracy, $\psi_{H} = |\pm 180°|$, that is involved in a three-bond separated $^{1}H_{\alpha}(i)$–$^{15}N(i+1)$ dipolar interaction is removed by incorporating an additional two-bond separated $^{1}H_{\alpha}(i)$–15N(i) dipolar interaction. Because the REDOR dephasing curves thus obtained show a ψ-torsion angle dependency, it must be possible to differentiate between major conformational structures possessing sufficiently different ψ-torsion angles based on the experimental REDOR dephasing curve of the three-spin system, $^{15}N(i)$–$^{1}H_{\alpha}(i)$–^{15}N($i+1$). Demonstrated in a separated plot shown on the bottom of Fig. 3A are the simulated REDOR dephasing curves for the $^{15}N(i)$–$1H_{\alpha}(i)$–15N($i+1$) spin system involved in α-helix (ψ = −47°) and β-sheet (ψ = 135°) structures. These two curves are significantly different at the longer mixing times (>2.4 ms). Even in the region with shorter mixing times (<2.0 ms), where an experimental observation of a REDOR dephasing curve is more reliable, the difference in the dephasing curves evidenced is far beyond an ambiguity a typical experimental error associated with an experimental REDOR dephasing curve with sufficient S/N ratio would impose. It is also predicted that the $^{15}N(i)$–$^{1}H_{\alpha}(i)$–$^{15}N(i+1)$ spin system may distinguishe the β-turn type-I structure against the type-II structure as explained in the Supplementary Fig. 2C. Based on the extensive simulations including many other peptide geometries possessing different secondary structures (Table 1), we reached to a general conclusion that while some overlap will be unavoidable among the dephasing curves from secondary structures possessing similar ranges of conformational angles (e.g. α-helix (ψ = −47°) and 3_{10}-helix (ψ = −26°); antiparallel (ψ = 135°) and parallel (ψ = 120°) β-sheets), the dephasing curve for the general case of an α-helical torsion angle is distinguishable from that of β-sheet torsion angle. Furthermore, when a site-specific resolution of $^{13}C_{\alpha}$ peak is provided, this method might be useful for determining multiple ψ-torsion angles of alanine-like residues in an extensively/uniformly ^{13}C-/^{15}N-labeled peptide/protein.

To test the validity of employing an effective $^{15}N(i)$–$^{1}H_{\alpha}(i)$–^{15}N($i+1$) system for the analysis of experimental $^{1}H^{C}_{\alpha}$—^{15}N REDOR data from a uniformly ^{15}N-labeled peptide or protein, additional nearby $^{1}H_{\alpha}(i)$–$^{15}N(i-1)$ and $^{1}H_{\alpha}(i)$–$^{15}N(i+2)$ interactions are included to the $^{1}H_{\alpha}(i)$–$^{15}N(i)$ and $^{1}H_{\alpha}(i)$–$^{15}N(i+1)$ interactions, forming an extended $^{1}H^{C}_{\alpha}$—$^{15}N_4$ spin system. These additional couplings vary depending on the (ϕ, ψ) torsion angle sets defined over three adjacent $i-1$, i, and $i+1$th residues. Various $^{1}H_{\alpha}(i)$–15N(y) ($y = i-1$, $i+1$, and $i+2$) distances and their relative angles with respect to the strongest $^{1}H_{\alpha}(i)$–$^{15}N(i)$ coupling are reported in the Supplementary Table 1 for the various types of secondary structures, such as α-helical, 3_{10}-helical, antiparallel β-sheet, parallel β-sheet, and β-turn types I and II structures. The dipolar coupling strengths of $^{1}H_{\alpha}(i)$–$^{15}N(i-1)$ and $^{1}H_{\alpha}(i)$–$^{15}N(i+2)$ spin pairs found in these secondary structures are in the range of 64–175 Hz, which are about 4.1–11.2% of the major $^{1}H_{\alpha}(i)$–$^{15}N(i)$ coupling strength. These dipolar interactions can safely be ignored in the REDOR analysis for initial REDOR mixing periods because the dipolar coupling strengths of these spin pairs are less than or comparable to 10% of that of $H_{\alpha}(i)$–N(i) and be effectively truncated [28]. More details of considering $^{1}H^{C}_{\alpha}$—$^{15}N_4$ spin system are included in the Supporting information.

Similarly, we have tested another three spin system, $C'(i-1)$–$1H_{N}(i)$–$C'(i)$, in a uniformly ^{13}C-labeled peptide system to test its validity in determining ϕ-torsion angles of major secondary structure. To utilize this spin system a selective irradiation scheme must be incorporated along the carbon channel to invert only carbonyl carbons. The proton echo signal of amide hydrogen must be encoded indirectly along the nitrogen signal based on a short CP. Since it involves dipolar coupling between the hydrogen and carbon nuclei, the dipolar coupling strengths involved in the spin system are more stronger than the previous case, and a REDOR S/S_0 curve obtained from this spin system dephases more rapidly as can be seen in Fig. 3B. As is seen in Fig. 3B, S/S_0 REDOR dephasing curves from major secondary structures, such as α-helix and β-sheet, are distinguishable. Because one has to accommodate for the two Gaussian π-pulses which possess significantly wider pulse durations than simple π-pulses per rotor period, a slower spinning speed must be used to increase the length of the spinning rotor period. Since a S/S_0 curve from this spin system dephases faster than the case involving nitrogens, it would impose a limitation in its use for practical applications.

Finally, we have tested the finite pulse effect and the influence of relative tensor orientations between the ^{15}N CSA tensors and ^{1}H–$^{15}N_2$ dipolar vectors in S/S_0 curves. The known magnitude of ^{15}N CSA tensor values [27] were incorporated in our REDOR simulations with adjustable relative tensor orientations. Fig. 4A shows the S/S_0 REDOR dephasing curves using π-pulses along the irradiation channel whose width are infinitely narrow, 5, 10, and 20 μs, under a 12 kHz of spinning speed. As is clear from Fig. 4A, the influence of the finite π-pulse effect is very significant particularly at a pulse power less than ω_1 = 50 kHz (width of the π-pulse is 10 μs), therefore, one needs to specify an exact π-pulse width in the brute-force numerical simulations. The S/S_0 curves for the α-helix and β-

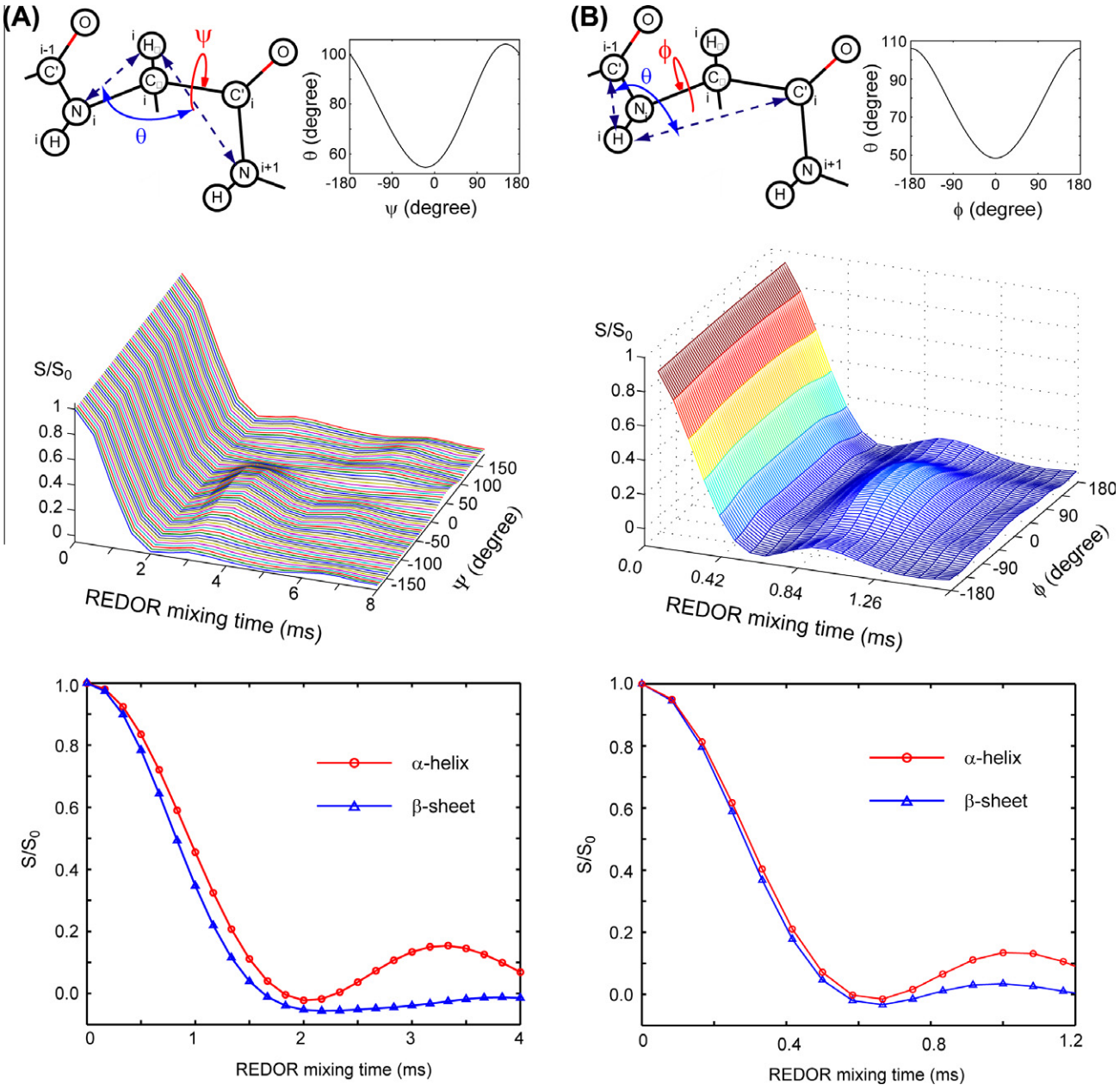

Fig. 3. Simulations of S/S_0 REDOR dephasing curves of three-spin systems, $^{15}N(i)$–$^{1}H_{\alpha}(i)$–$^{15}N(i+1)$ (A) and $^{13}C'(i-1)$–$^{1}H_{N}(i)$–$^{13}C'(i)$ (B), obtained by varying the ψ- (A) and ϕ-torsion (B) angles. The θ angle, 3-D S/S_0 REDOR dephasing plot, and representative S/S_0 REDOR dephasing curves for α-helix ($\psi = -47°$, $\phi = -57°$) and parallel β-sheet ($\psi = 120°$, $\phi = -119°$) structures for both spin systems are shown by varying either ψ- (A) or ϕ-torsion (B) angle in the range of $-180°$ to 180°. Simulations were performed utilizing a MAS rate at 12 kHz, 5 μs 180° X-pulses, and known tensor values of $^{13}C'$ and ^{15}N CSA tensor parameters. The relative tensor orientations between CSA and ^{1}H–X dipolar vector were ignorable. The FSLG scaling factor, 0.577, was considered for the strength of dipolar couplings. Homonuclear ^{1}H–^{1}H dipolar couplings are ignored in the simulations.

sheet structures start to oscillate at the longer mixing time due to the influence of ^{15}N CSA when 40 μs of π-pulses are used. The isotropic offset frequencies considered for $^{15}N(i)$ and $^{15}N(i+1)$ were arbitrarily assigned to ±5 ppm.

Fig. 4B shows an invariance in S/S_0 REDOR dephasing curves due to the changes in the relative CSA tensor orientations of ^{15}N nuclei with respect to the ^{1}H–^{15}N dipolar vector. The same simulation parameters were used as before, with $\omega_1(^{15}N) = 100$ kHz. Compared in Fig. 4B are S/S_0 dephasing curves obtained with $\alpha_1^{cs} = \alpha_2^{cs} = \beta_1^{cs} = \beta_2^{cs} = 0°$ (red circle) and $\alpha_1^{cs} = \alpha_2^{cs} = \beta_1^{cs} = \beta_2^{cs} = 90°$ (blue cross). As these two curves from different ^{15}N CSA tensor orientations are the same, we can conclude that the influence of relative tensor orientations between the ^{15}N CSA and ^{1}H-^{15}N dipolar vectors is ignorable.

4. Experimental results and discussion

The feasibility of detecting a site-specific ψ-torsion angle was tested on a ^{13}C-/^{15}N-labeled model system consisting of a three amino acid peptide Gly–[U–^{13}C, ^{15}N]Ala–[U–^{13}C, ^{15}N]Leu (^{13}C/^{15}N labeling purity: 98.0%) that is diluted to 18.0% in natural abundance Gly–Ala–Leu, which was subsequently recrystallized according to the literature procedure [26]. This is a good model compound because its X-ray crystal structure is known [26]—the alanine residue positioned in the center of the tripeptide possesses an α-helical torsion angle ψ(Ala) = $-39°$ (see the inset in Fig. 5C). REDOR dephasing signals (S) and reference signals (S_0) were recorded with and without ^{15}N π pulses, respectively. An example of a set of S and S_0 ^{13}C spectra, measured at the REDOR mixing time

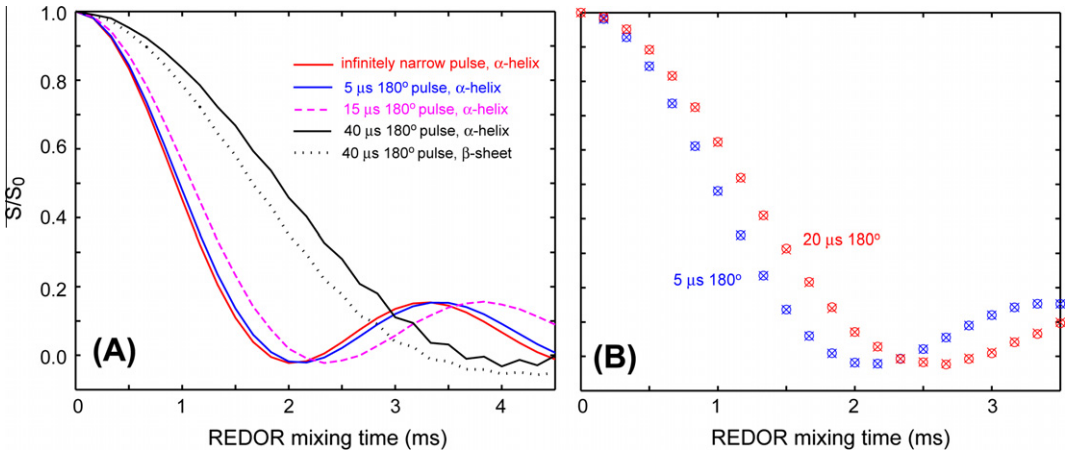

Fig. 4. Finite pulse effect (A) and the influence of the relative tensor orientations between the CSA of ^{15}N and ^{1}H–^{15}N dipolar vector (B). In (A), S/S_0 REDOR simulations were carried out for a ^{15}N(i)–^{1}H$_\alpha$(i)–^{15}N($i+1$) spin system with $\psi(i) = -47°$ (α-helix) and 135° (β-sheet). Known ^{15}N's CSA values were utilized in the simulations, assuming coinciding CSA and dipolar tensor orientations. The pulse width of the 180° rf pulses applied along the ^{15}N channel was assumed to be infinitely narrow (solid red; α-helix), 5 μs (solid blue; α-helix), 15 μs (dashed pink; α-helix), 40 μs (solid black; α-helix), and 40 μs (solid dot; β-sheet). In (B), the same spin system as (A), with α-helical torsion angle and 5 μs (blue) and 20 μs (red) of 180° ^{15}N pulses, was used in the simulations assuming coinciding (circle) and orthogonal (cross) ^{1}H–^{15}N dipolar and ^{15}N CSA tensors. (For interpretation of the references to colour in this figure legend, the reader is referred to the web version of this article.)

0.688 ms, is shown in Fig. 5A. The expected REDOR dephasing phenomenon on the $^{1}H_\alpha$ of Ala residue is clearly visible along the indirectly detected C_α(Ala) signal on the S spectrum. The experimental S_0 curve of the $^{1}H_\alpha$ signal of alanine over all REDOR mixing times is also shown in Fig. 5B to indicate the influence of the apparent T_2 relaxation on the signal dephasing which is determined by the efficiency of FSLG ^{1}H–^{1}H dipolar decoupling. A key component of this technique for improving the signal-to-noise ratio is to ensure the evolution of a ^{1}H magnetization during the REDOR mixing time with a sufficiently long T_2 relaxation time. The signal dephasing due to T_2 relaxation is common in both S and S_0 spectra. Thus, in the S/S_0 fraction, the signal dephasing is purely due to the ^{1}H–^{15}N heteronuclear dipolar interactions.

A further signal correction is required in the experimental S/S_0 curve (Fig. 5C) to reflect the NMR signal intensities in S and S_0 spectra due to the contributions from the natural abundance signals. To

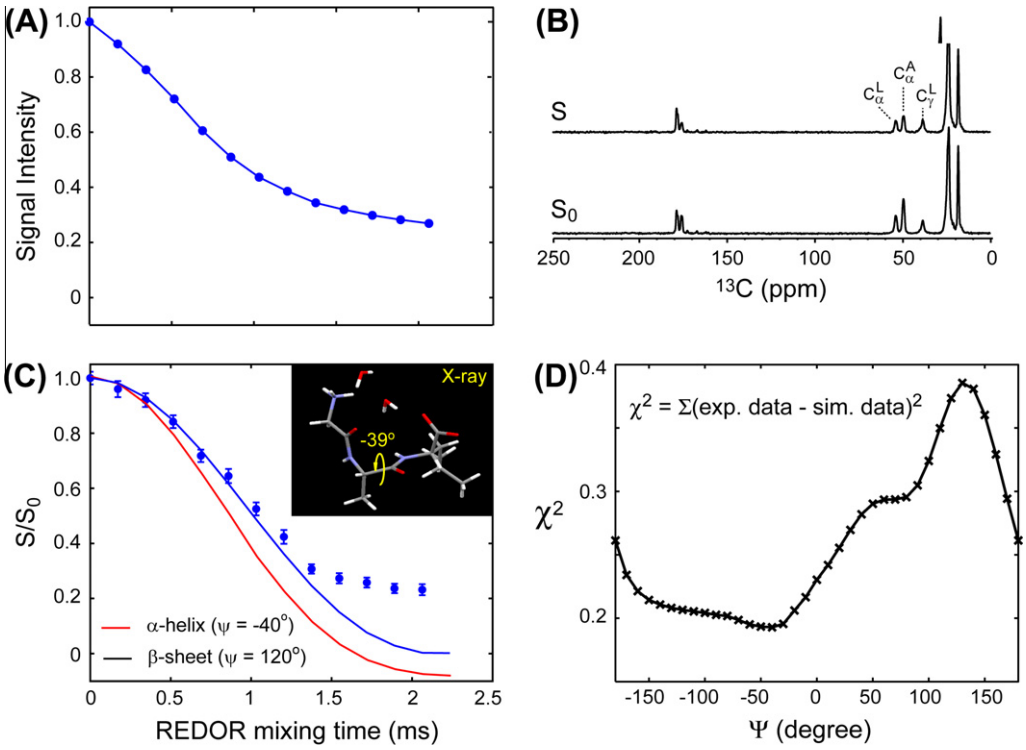

Fig. 5. (A) S and S_0 spectra of ^{13}C-/^{15}N-labeled GAL obtained at 0.688 ms REDOR mixing time. (B) Experimental $^{1}H_\alpha$ S_0 T_2 decay curve of the alanine residue of GAL. The length of the apparent T_2 relaxation time reflects the FSLG decoupling efficiency. (C) Experimental $^{1}H_\alpha$–$^{15}N_2$ S/S_0 dephasing curve of the alanine residue of GAL and simulation curves obtained by assuming α-helical and β-sheet torsion angles. Experimental data (blue dots, with error bars) fit well to the simulated dephasing curve for an α-helix with a ψ torsion angle of −40° (blue line). A prediction based on a β-sheet secondary structure (ψ = 120°) is also included for a comparison (black line). The X-ray determined ψ-torsion angle of alanine is −39°, as shown in the inset. (D) Total squared deviations between experimental and simulated data by means of squared noise (χ^2) as a function of the torsion angle ψ for the alanine residue of GAL. (For interpretation of the references to colour in this figure legend, the reader is referred to the web version of this article.)

remove the signal portion that contributes only to the S_0 signal due to the presence of $^{13}C_\alpha$–$^1H_\alpha$–^{14}N combinations in the sample, which is relatively about 0.0126 (from the labeled peptide: 0.980 (^{13}C) × 0.99985 (^1H) × 0.020(^{14}N) × 0.180 [the dilution factor of labeled peptide] = 0.00353; from the natural abundance peptide: 0.0111 (^{13}C) × 0.99985 (^1H) × 0.9963 (^{14}N) × 0.820 = 0.00907). The portion of $^{13}C_\alpha$–$^1H_\alpha$–^{15}N combinations that contribute to both S and S_0 signals is 0.173 (from the labeled peptides: 0.980 (^{13}C) × 0.99985 (^1H) × 0.980(^{15}N) × 0.180 = 0.173; the portion from the natural abundance peptides is negligible). Here we considered only the major spin pair $^1H_\alpha(i)$–$^{15}N(i)$ that dominates the S/S_0 REDOR dephasing for simplicity. The fraction that does not dephase is therefore 0.0126/(0.0126 + 0.173) = 0.0679. Thus, the true S/S_0 REDOR dephasing signal must be $(S - 0.0679S_0)/(S_0 - 0.0679S_0)$.

Shown in Fig. 5C is the corrected experimental S/S_0 dephasing curve along with simulated dephasing curves. Error bars are included in the experimental data by calculating $(S/S_0) \times (1/\mathrm{SINO} + 1/\mathrm{SINO}_0)$ for each point, where SINO and SINO_0 are the signal-to-noise ratio of S spectrum and S_0 spectrum, respectively. Within the initial region of the REDOR dephasing curve, the corrected S/S_0 values obtained experimentally match well with simulations using $\psi \approx -40°$. Also included is a simulation based on a β-sheet secondary structure ($\psi = 120°$) for comparison. Fig. 5D shows the c2 deviation between experiments and simulations as a function of y angle that is assumed in the simulation. The best-fit result is around $\psi = -40°$ with an error range within ±30°. Interestingly, no reflection symmetry is observed in Fig. 5D, due to the non-symmetric nature of the three-spin system, $^{15}N(i)$–$^1H_\alpha(i)$–$^{15}N(i+1)$, on the rotation of $\psi(i)$ (see also Fig. 3A). We have included the FSLG scaling factor (0.57) for considering ^1H–^{15}N dipolar coupling strengths in our REDOR data analysis. The best fit simulation data with assuming an α-helical ψ-torsion angle is in reasonable agreement with the known crystal structure of GAL ($\psi_{\mathrm{Ala}} = -39°$) [26]. Deviations of experimental points from the simulation at long mixing times would be attributed to errors associated with experimental imperfections, such as insufficient ^1H–^1H dipolar decoupling, *rf* inhomogeneity, and finite pulse effects or pulse imperfections, which are not able to be compensated. These errors would be accumulated when the REDOR mixing time increases. This limitation would be particularly severe when it is associated with the lower signal-to-noise ratio of a S/S_0 signal that approaches to zero at a longer mixing time. Still, a good agreement at short mixing times, which is normally the time region of most interest in REDOR data analysis, supports the efficacy of our REDOR method for determining torsion angles.

Though it possesses a relatively poor angular resolution, the potential usefulness of this approach is a possibility of providing a sequential ψ-torsion angle measurement if the site-specificity of C_α signals is provided. Thus, the resolution of C_α carbons is a limiting factor to be applied a uniformly or extensively ^{13}C-labeled sample system. Practically, a peptide or protein sample must be recrystallized for obtaining the highest $^{13}C_\alpha$ spectral resolution. A small, uniformly-$^{13}C/^{15}N$-labeled peptide sample or a selectively labeled protein sample is practically an optimal sample system for this method. Directly bonded $^{13}C_\alpha$–$^{13}C_\beta$ or $^{13}C_\alpha$–$^{13}C'$ dipolar interactions in a uniformly ^{13}C-labeld sample system would also impose a limitation for obtaining well resolved C_α peaks. A ^{13}C-/^{15}N-labeled sample system is superior to the only ^{13}C-labeled sample system for obtaining high-resolution $^{13}C_\alpha$ signals due to the absence of a quadrupole-dipole cross-correlation in $^{13}C_\alpha$–^{14}N pair that does not be averaged away by magic-angle sample spinning [30]. When a protein sample is examined, an extension to the two-dimensional (2D) $^{15}N/^{13}C'$ or $^{15}N/^{13}C_\alpha$ correlation experiment as indicated in Fig. 1A would be helpful to increase the resolving power of a spectrum in most practical cases.

5. Conclusion

Spin systems involving $^1H_\alpha$ or ^1H_N nuclei, such as $^1H_\alpha(i)$–$^{15}N(i+1)$, $^1H_\alpha(i)$–$^{13}C'(i-1)$, and $^1H_N(i)$–$^{15}N(i)$, are explored for determining site-specific $\psi(i)$- or $\phi(i)$-torsion angles in a selectively ^{15}N- and/or ^{13}C-labeled peptide system. An indirect detection scheme via either ^{15}N or $^{13}C_\alpha$ nuclei can conveniently be utilized to encode the signals of ^1H–X (X = ^{13}C or ^{15}N) REDOR spectroscopy. For a uniformly or extensively ^{13}C-/^{15}N-labeled peptide/protein sample system, a $^1H_\alpha^C$—N_2 REDOR scheme is demonstrated for measuring multiple, site-specific $\psi(i)$-torsion angles of alanine-like residues. This method has a potential to determine $\psi(i)$-torsion angles with an angular precision that determine major secondary structures: it distinguishes α-helix against β-sheet structures or turn type-I structure against type-II structure, etc. Although it provides a limited capability to distinguish between the ψ-torsion angles representing α-helix and 3_{10}-helix structures, or ψ-torsion angles representing antiparallel β-sheet and parallel β-sheet structures, this method can still be a very powerful tool for residue-specific ψ-torsion angle determination of a uniformly/extensively ^{13}C-/^{15}N-labeled peptide/protein because a sequential, site-specific ψ-torsion angle determination is feasible.

The finite-pulse duration of π-pulses applied along the irradiation channel must be considered explicitly in the simulation of REDOR curves. However, complications due to the presence of chemical shift anisotropies (CSAs) of ^{15}N nuclei and their relative tensor orientations to the ^1H–^{15}N dipolar pairs involved were negligible [21]. A $^1H_\alpha$ spin of an alanine-like residue in a peptide sequence is well separated from $^{15}N(i-1)$ and $^{15}N(i+2)$ etc. that it forms an effective N(i)–$^1H_\alpha i$–N($i+1$) spin system.

Acknowledgment

This research was supported by the NSF (CHE-0541764).

Appendix A. Supplementary material

Supplementary data associated with this article can be found, in the online version, at doi:10.1016/j.jmr.2011.08.019.

References

[1] K. Schmidt-Rohr, Torsion angle determination in solid ^{13}C-labeled amino acids and peptides by separated-local-field double-quantum NMR, J. Am. Chem. Soc. 118 (1996) 7601.
[2] K. Schmidt-Rohr, A double-quantum solid-state NMR technique for determining torsion angles in polymers, Macromolecules 29 (1996) 3975–3981.
[3] X. Feng, M. Edén, A. Brinkmann, H. Luthman, L. Eriksson, A. Gräslund, O.N. Antzutkin, M.H. Levitt, Direct determination of a peptide torsional angle ψ by double-quantum solid-state NMR, J. Am. Chem. Soc. 119 (1997) 12006–12007.
[4] P.R. Costa, J.D. Gross, M. Hong, R.G. Griffin, Direct determination of a peptide torsional angle ψ by double-quantum solid-state NMR, Chem. Phys. Lett. 280 (1997) 95.
[5] X. Feng, Y.K. Lee, D. Sandstrom, M. Edén, H. Maisel, A. Sebald, M.H. Levitt, Direct determination of a molecular torsional angle by solid-state NMR, Chem. Phys. Lett. 257 (1996) 314.
[6] M. Hong, J.D. Gross, R.G. Griffin, Site-resolved determination of peptide torsion angle φ from the relative orientations of backbone N–H and C–H bonds by solid-state NMR, J. Phys. Chem. B 101 (1997) 5869–5874.
[7] Y. Ishii, T. Terao, M. Kainosho, Relayed anisotropy correlation NMR: determination of dihedral angles in solids Original Research Article, Chem. Phys. Lett. 256 (1996) 133.
[8] P.V. Bower, N. Oyler, M.A. Mehta, J.R. Long, P.S. Stayton, G.P. Drobny, Determination of torsion angles in proteins and peptides using solid state NMR, J. Am. Chem. Soc. 121 (1999) 8373–8375.
[9] F.J. Blanco, R. Tycko, Determination of polypeptide backbone dihedral angles in solid state NMR by double quantum ^{13}C chemical shift anisotropy measurements, J. Magn. Reson. 149 (2001) 131.
[10] J.C.C. Chan, R. Tycko, Solid-state NMR spectroscopy method for determination of the backbone torsion angle ψ in peptides with isolated uniformly labeled residues, J. Am. Chem. Soc. 125 (2003) 11828–11829.

[11] J.R. Long, J.L. Dindot, H. Zebroski, S. Kiihne, R.H. Clark, A.A. Campbell, P.S. Stayton, G.P. Drobny, A peptide that inhibits hydroxyapatite growth is in an extended conformation on the crystal surface, Proc. Natl. Acad. Sci. USA 95 (1998) 12083.
[12] N. Sinha, M. Hong, X-^{1}H rotational-echo double-resonance NMR for torsion angle determination of peptides, Chem. Phys. Lett. 380 (2003) 742.
[13] I. Sack, Y.S. Balazs, S. Rahimipour, S. Vega, Solid-state NMR determination of peptide torsion angles: applications of ^{2}H-dephased REDOR, J. Am. Chem. Soc. 122 (2000) 12263.
[14] S. Wi, N. Sinha, M. Hong, Long-range ^{1}H-19F distance measurement in peptides by solid-state NMR, J. Am. Chem. Soc. 126 (2004) 12754.
[15] Y. Mou, T.W.T. Tsai, J.C.C. Chan, Determination of the backbone torsion psi angle by tensor correlation of chemical shift anisotropy and heteronuclear dipole–dipole interaction, Solid State Nucl. Magn. Reson. 31 (2007) 72.
[16] J.C.C. Chan, R. Tycko, Recoupling of chemical shift anisotropies in solid-state NMR under highspeed magic-angle spinning and in uniformly ^{13}C-labeled systems, J. Chem. Phys. 118 (2003) 8378.
[17] T. Gullion, J. Schaefer, Rotational-echo double-resonance NMR, J. Magn. Reson. 81 (1989) 196.
[18] T. Gullion, J. Schaefer, Elimination of resonance offset effects in rotational-echo double-resonance NMR, J. Magn. Reson. 92 (1991) 439.
[19] N. Sinha, M. Hong, X-H-1 rotational-echo double-resonance NMR for torsion angle determination of peptides, Chem. Phys. Lett. 380 (2003) 742.
[20] K. Schmidt-Rohr, M. Hong, Measurements of carbon to amide-proton distances by C–H dipolar recoupling with N-15 NMR detection, J. Am. Chem. Soc. 125 (2003) 5648.
[21] R. Fu, Measurement of N-15–H-1 bond lengths by rotational-echo double-resonance NMR spectroscopy, Chem. Phys. Lett. 376 (2003) 62.
[22] M. Lee, W.I. Goldburg, Nuclear-magnetic-resonance line narrowing by a rotating rf field, Phys. Rev. 140 (1965) A1261.
[23] B.J. van Rossum, C.P. de Groot, V. Ladizhansky, S. Vega, H.J.M. de Groot, A method for measuring heteronuclear (^{1}H–^{13}C) distances in high speed MAS NMR, J. Am. Chem. Soc. 122 (2000) 3465.
[24] A. Bielecki, A.C. Kolbert, H.S.M. de Groot, R.G. Griffin, M.H. Levitt, Frequency-switched Lee–Goldburg sequences in solids, Adv. Magn. Reson. 14 (1990) 111.
[25] W.K. Rhim, D.D. Elleman, R.W. Vaughan, Analysis of multiple pulse NMR in solids, J. Chem. Phys. 59 (1973) 3740.
[26] S. Chaturvedi, K. Go, R. Parthasarathy, A sequence preference for nucleation of helix – crystal structure of Gly-L-Ala-L-Val and Gly-L-Ala-L-Leu: Some comments on the geometry of leucine zippers, Biopolymers 31 (1991) 397.
[27] C.H. Wu, A. Ramamoorthy, L.M. Gierasch, S.J. Opella, Simultaneous characterization of the amide ^{1}H chemical shift, ^{1}H–^{15}N dipolar, and ^{15}N chemical shift interaction tensors in a peptide bond by three-dimensional solid-state NMR spectroscopy, J. Am. Chem. Soc. 117 (1995) 6148.
[28] C.A. Fyfe, A.R. Lewis, Investigation of the viability of solid-state NMR distance determinations in multiple spin systems of unknown structure, J. Phys. Chem. B 104 (2000) 48.
[29] F.G. Vogt, J.M. Gibson, S.M. Mattingly, K.T. Mueller, Determination of molecular geometry in solid-state NMR: rotational-echo double resonance of three-spin systems, J. Phys. Chem. B 107 (2003) 1272.
[30] R.K. Harris, A.C. Olivieri, Quadrupolar effects transferred to spin-magic-angle spinning spectra of solids, Prog. NMR Spectrosc. 24 (1992) 435.